ingegneria sismica
International Journal of Earthquake Engineering
Anno XXXV – Num.4

MODAL PARAMETER IDENTIFICATION OF PROGRESSIVELY DAMAGED REINFORCED CONCRETE FRAMES WITH VARIOUS INFILL CONDITIONS

Ozgur Ozcelik[1,2], Umut Yucel[1], Erkan Durmazgezer[1]

[1]Department of Civil Engineering, Dokuz Eylul University, Izmir, Turkey

[2]Currently Researcher at Department of Structural Engineering, University of California, San Diego

SUMMARY: *In this paper, modal identification results of half-scale, single-bay, single-story three reinforced concrete (R/C) frames with different infill conditions are presented. The frames were tested along their in-plane directions under gradually increasing quasi-static cyclic loading. At each predetermined drift level, ambient vibration and white-noise tests were conducted on the frames for the purpose of identifying their modal parameters. The modal identification results are correlated with detailed visual damage inspections. This paper aims to investigate (i) the evolution of the estimated modal parameters as a function of increasing structural damage, (ii) the performance of various output-only system identification methods in identifying modal parameters of damaged frames, (iii) the identification results obtained by using different excitation types having different amplitude levels, and (iv) the influence of different types of infills on the induced damage, and therefore to assess the effects of increasing infill damages on the modal identification results.*

KEYWORDS: *reinforced concrete frames, quasi-static testing, infilled frames, linear shaker tests, modal parameter identification, operational modal analysis*

1 Introduction

Structural health monitoring (SHM) has become an attractive and popular tool for assessing state and health of civil engineering structures. Structural damage alters mass, stiffness, and energy dissipation characteristics of structural systems. These changes result in detectable variations in systems' vibration characteristics. Detecting these variations is the main principle of vibration-based SHM [Doebling *et al.*, 1998, Sohn *et al.*, 2003]. The operational modal analysis (OMA) belongs to the system identification discipline which is widely used to estimate vibration characteristics of structures (i.e., natural vibration frequencies, mode shapes, and damping ratios, a.k.a. modal parameters) using only-output response data. These tools are generally utilized to identify modal parameters of structures idealized as equivalent viscously damped linear elastic time-invariant systems. A fundamental assumption in OMA techniques is that the structure to be investigated is excited by random broad-band excitation (i.e., having white-noise (WN) characteristics), or at least having band-limited WN characteristics. Broad-band excitation enables various structural modes to be excited sufficiently, and it is also necessary for avoiding the system to be driven at a specific frequency.

Corresponding author: Ozgur Ozcelik, Department of Civil Engineering, Dokuz Eylul University, Turkey.
Email: ozgur.ozcelik@deu.edu.tr

Infill walls inside R/C frames have long been considered as nonstructural members by many researchers, but nevertheless there have been numerous attempts for classifying them as structural members and including their effects in nonlinear response analysis [Lima *et al.*, 2017]. There are numerous studies available on modal identification of reinforced concrete (R/C) structures with different infill conditions tested under dynamic conditions in the literature. Some of these studies are briefly reviewed here. Moaveni *et al*. (2012) performed modal identification study on a progressively damaged three-story building using input-output vibration data. Structural damage stated at different damage levels were determined by a sensitivity-based model updating method. In another study by Moaveni *et al*. (2010), modal parameters of a seven-story R/C building slice tested on a shake table were estimated under progressively increasing damage levels. To do that at each damage level, low amplitude WN tests have been used. Ji *et al*. (2010) imposed various levels of realistic damage conditions by the NIED E-Defense shake table in Japan. Using frequency response functions (FRF) and auto-regressive exogenous input method (ARX), modal parameters of a four-story real-size R/C building were identified at different damage levels. Belleri *et al*. (2014) performed damage identification work on a 3-story 1/2-scale precast concrete parking structure subjected to various ground motions on a shake table. The recorded input-output data was used with deterministic-stochastic subspace method for modal identification purpose. Astroza *et al*. (2016) identified modal parameters of a real-size five-story fixed-base R/C building subjected to a sequence of earthquake ground motions with increasing intensities on a large outdoor shake table. The recorded data from WN and ambient vibration (AV) tests were processed by two input-output and three output-only system identification methods. Changes in the modal parameters as a function of increasing damage were reported. Stavridis *et al*. (2012) performed a series of shake table tests on a 2/3-scale R/C frame with un-reinforced solid masonry brick infills. Series of dynamic tests, including AV, WN, and historical earthquake records with increasing intensities, were performed. One of the objectives of the study was to determine the fundamental frequency of the frame experiencing progressively increasing damage. Another increasingly attractive area of research is the infill wall out-of-plane damage and its effect on infill wall's in-plane behavior [Donà *et al.*, 2017]. The in-plane and out-of-plane interaction further complicates the issue of dynamically characterizing R/C frames with infill walls.

This work aims to present modal parameter estimations of single-bay single-story half-scale three different R/C frames with different infill conditions. The frames were quasi-statically tested under progressively increasing in-plane drifts and then dynamically tested at the end of some of these drift levels. At different drift levels, therefore at different damage states, AV and WN (with different excitation amplitudes) tests were conducted for modal parameter identification. An electro-dynamic shaker, positioned on top of the slab, was used to perform WN tests. Three different output-only system identification methods, namely, Multiple-Reference Natural Excitation Technique combined with Eigensystem Realization Algorithm (MNExT-ERA), Data-Driven Stochastic Subspace Identification (SSI-DATA), and Enhanced Frequency Domain Decomposition (EFDD) are used with the recorded response data at different damage states. A comparative study is performed for different frames at different damage levels. Detailed visual damage inspections, made during quasi-static tests (i.e., at discrete damage states), and their evolution with respect to increasing drift levels are coupled with the corresponding modal identification results. This allows correlation studies to be made among identified modal parameters, damage types, their locations, and their extent.

Effects of different infill walls on the identification results at different damage states are also reported. Also, the presented results will be later used for finite element model updating based damage identification purpose.

2 Description of R/C Frames and Test Program

One bare (i.e., no infill) and two infilled half-scale single-bay single-story R/C frames with partial slabs were tested under quasi-static loading. The quasi-static loading was applied along the frames' in-plane direction. The average 28^{th} day compressive strength of the concrete used is ~38 MPa, and the nominal yield strength of the steel bars is 420 MPa. The column and beam elements have cross-sectional dimensions of 15 cm x 25 cm. The frames have a height of 150 cm measured from foundation top to slab top, and center-to-center column span was 225 cm. All frames have 6 cm thick partial slabs. The schematic view and rebar detailing of the frames are presented in Figures 1(a) and (b), respectively. A vertical load of approximately 10% of columns' axial load capacity was applied on each column by two separate but parallel connected hydraulic pistons. This load represents the weight of the upper stories. The pressure level in these pistons was monitored during the tests by a manometer attached to the supply line to check the level of axial load applied on the columns. In addition to the axial load applied by these pistons, 4 concrete pads (each weighing 1.38 kN) and 16 steel plates (each weighing 0.18 kN) were placed on the slab for representing gravity loads on the beams. In-plane displacement was applied to the R/C frames by a hydraulic actuator with displacement controller. The actuator was attached on the frames at the slab level (see Figure 1(c)). The actuator used is a double-acting actuator capable of applying cyclic displacements.

Two different types of brick units namely standard and locked bricks, as shown in Figure 2, were used to build the infill walls. The main difference between these bricks is that the former one uses mortar on the bed and head-joints (standard brick), and the latter one does not use mortar on any of these joints (locked brick). The locked bricks lock into each other while enabling sliding motion along their in-plane direction (along the strong axis of the R/C frames) due to their mortar-less feature. This novel feature of the brick enables low-to-moderate level panel action to develop within frame systems, and therefore has the potential of preventing soft or weak story mechanism [Misir *et al.*, 2012]. The out-of-plane stability (along the weak axis of the R/C frames) is provided by the brick's internal locking feature. Mortar was used at all brick-to-brick and brick-to-frame interfaces for the infill wall constructed with standard bricks whereas for the infill wall with locked bricks, mortar was used only at the brick-to-foundation interface. At the brick-to-beam interface, a foam-type material was used as is the case for real-life applications. The wall with locked bricks can be considered as a real non-structural member, since the wall itself has very low in-plane strength. Whereas in the standard brick case, the infill wall acts as a structural member at least until its maximum strength is reached, and from thereof it gradually loses its in-plane strength. These interpretations regarding the effects of infill walls, for both standard and locked infills, inside R/C frames are to be investigated through the modal identification work done at gradually increasing damage levels.

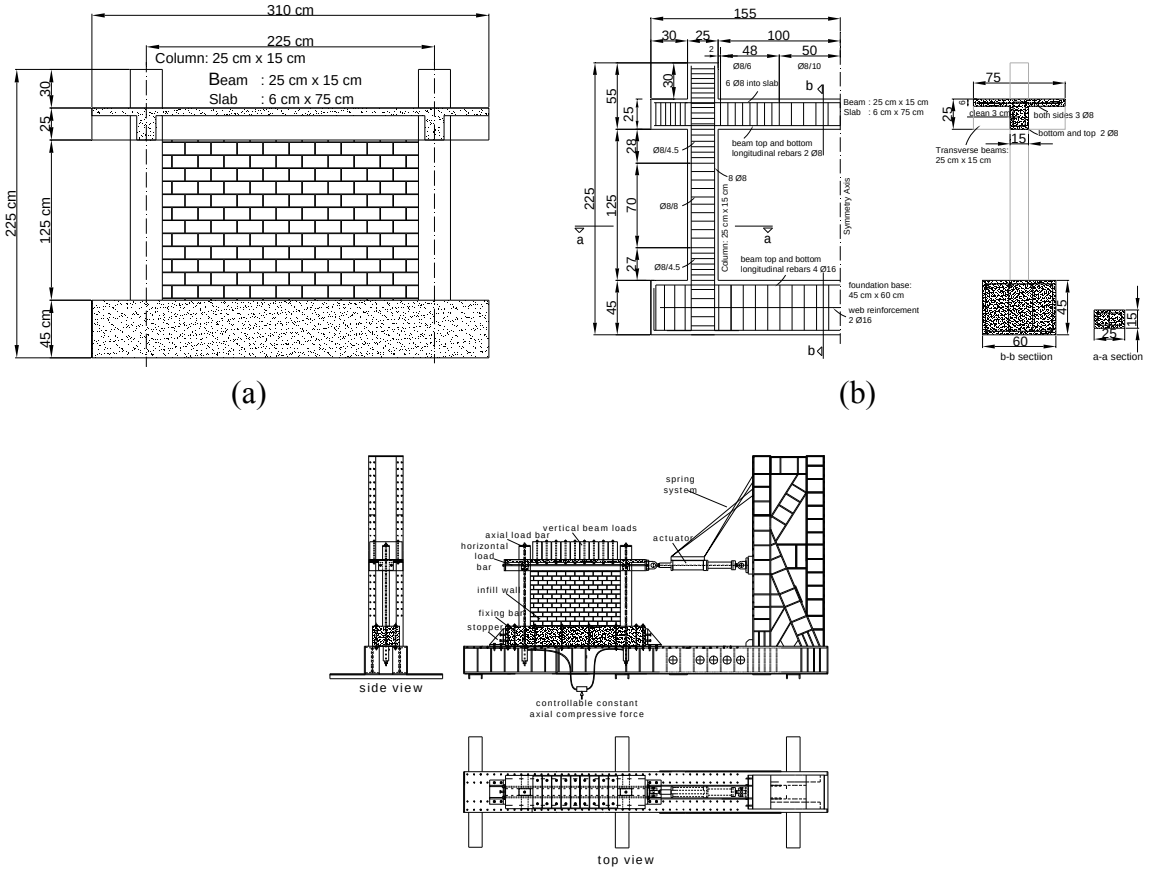

Figure 1 - (a) *Schematic View and* (b) *Reinforcing Details of the Frames*, (c) *Drawings of the Test Setup*

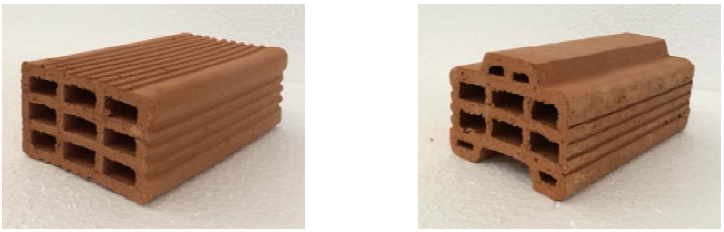

(a) (b)

Figure 2 - (a) *Standard and* (b) *Locked Type Bricks*

Types of infills used inside the test frames are shown in Table 1. Note that all the tests performed were single-cycle quasi-static tests where the displacement pattern for each test is based on ACI 374.1.05 (2005) and is shown in Figure 3. At the end of each pre-determined in-plane drift ratios: 0%, 0.2%, 0.5%, 1.0%, 1.4%, 2.2%, and 3.5% (i.e., at gradually increasing damage levels), a series of WN and AV tests were performed on the frames. These dynamic test points are indicated in Figure 3 with the circle symbol. Dynamic test points were selected so that significant changes in modal parameters as damage level increases can be captured.

Table 1 - *Infill Conditions of the Frames*

Frame #	Infill	Type of Masonry
F1	No	-
F2	Yes	Locked
F3	Yes	Standard

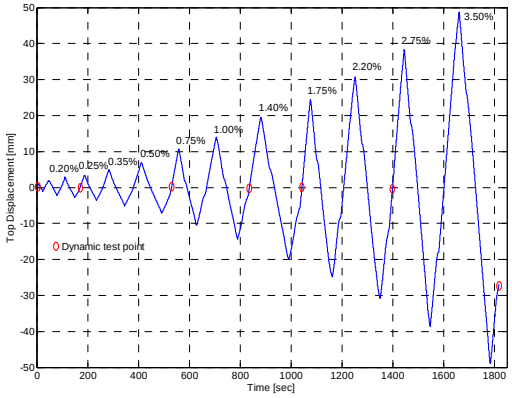

Figure 3 - *Single Cycle Displacement Pattern Imposed on the Frames*

The actuator was detached from the frames before AV and WN tests were performed. This was done to ensure that the restraining effect of the actuator on the specimen along the in-plane direction could be avoided. 12 minutes long AV and WN response data (7 sets for each specimen) at the end of the predetermined drift ratios were recorded at a rate of 250 Hz. Prior to performing modal identification work, the recorded time series were filtered between 0.5 – 100 Hz using a band-pass finite impulse response filter to increase estimation accuracy by focusing the estimation effort on the frequency range of interest.

For WN tests, an electro-dynamic shaker with an increased reaction mass positioned at the slab's mid-line (on top of the frames) was used for applying in-plane broad-band dynamic excitation on the R/C frames with an intention to excite in-plane mode(s). The input signal to the shaker, the same one was used for all tests, was designed so that it had a frequency bandwidth of 0.1 – 100 Hz. This bandwidth was deemed sufficiently broad-band to excite first few in-plane modes obtained based on preliminary numerical model studies. The signal amplitude was regulated manually by the gain knob of the signal amplifier unit; but was set to a fixed value once sufficiently high vibration response was observed. A control method called Offline Tuning Technique (OTT), a command shaping control strategy, was used for WN tests to improve the signal reproduction fidelity of the shaker in terms of both amplitude and frequency content [Yucel, 2014, Thoen and Laplace, 2004, Ozcelik *et al.*, 2015]. Implementation of a control strategy was necessary due to the fact that the shaker itself has no built-in controller. Therefore, OTT method, its details to be described in the following section, was used to achieve the desired broad-band characteristics of the input signal.

The frames were densely instrumented with 5 uni-axial and 4 tri-axial piezo-electric type accelerometers. Also, one uni-axial accelerometer was deployed on the electro-dynamic shaker's reaction mass for measuring the level of input excitation along the in-plane direction. Accelerometers used have ±5g amplitude range, frequency bandwidth of 0.25 Hz to 3000 Hz, sensitivity of 1000 mV/g. Three 18-bit A/D converters with 8 channels each, were used.

Multiple A/D modules were all synchronized. Spatial distribution of the accelerometers was decided based on the modal analysis results using the initial numerical model. Since the response of the structure is governed mainly by the modes in the frequency band of interest, sensor placement was performed by investigating the fundamental in-plane mode of the numerical model. The accelerometer stations with their positive polarities are shown in Figure 4. Additionally, 2 string potentiometers and 12 displacement transducers were used on the structural members (i.e., columns, beams, and infill walls) for response measurements during quasi-static testing. A general view of a test setup for one of the infilled frames is shown in Figure 5.

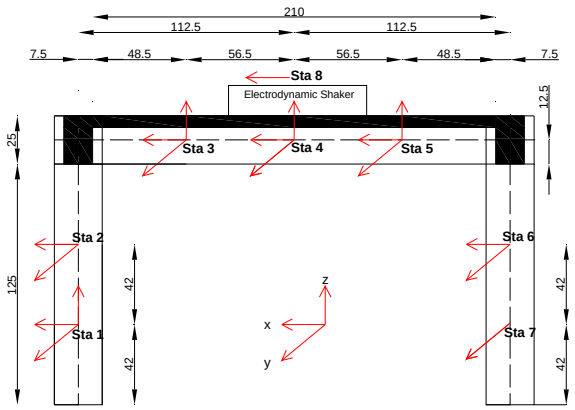

Figure 4 - *Electro-Dynamic Shaker on the Slab, and the Accelerometer Layout with Positive Polarities*

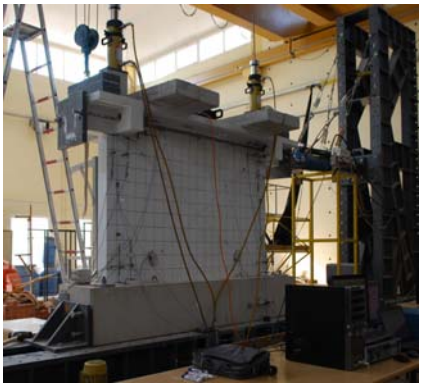

Figure 5 - *General View of a Test Setup with Sensors and other Test Equipment*

3 Increased Signal Fidelity by Offline Tuning Technique (OTT)

Frequency content of a dynamic excitation signal should cover a wide range of frequencies to excite a system's modes properly. Lack of frequency content for exciting some modes is an apparent drawback in modal identification applications. Therefore, it is important and desirable to excite dynamic systems with broad-band excitation signals so that the measured response data contains desired system dynamics. If a control algorithm is not used, the total forward transfer function estimation (i.e., estimated between the command and the achieved acceleration signals) of the electro-dynamic shaker clearly shows that the input signal cannot be reproduced properly in terms of both target amplitude and frequency content [Yucel, 2014, Twitchell and Symans, 2003]. In other words, there is a tracking error between the target (command) and the achieved (feedback) signals. This is known as the trajectory tracking problem [Luco *et al.*, 2010, Mota, 2011]. Solving this problem is essential for obtaining broad-band excitation signal, and therefore partially reducing estimation errors in modal parameter estimation process. The trajectory tracking problem of this particular shaker was remedied by using a command shaping method called the Offline Tuning Technique (OTT) [Yucel, 2014, Thoen and Laplace, 2004, Ozcelik *et al.*, 2015]. Based on this technique, the command acceleration signal, which has broad-band characteristics, is multiplied by the inverse of the total forward transfer function in the frequency domain, and then high-pass filtered to avoid large shaker motion surpassing the shaker's operational limits. The modified input signal obtained this way is transformed back to time domain by the inverse discrete

Fourier transform, and is used as the adjusted command input to the shaker. This way the achieved signal on the shaker platen would be in broad-band nature as the designed input signal. In this paper, the response data recorded from the WN tests where the OTT method is used will be denoted as "WN w/Offline" whereas the data recorded without the OTT method will be denoted as "WN wo/Offline".

4 Methods Used for Modal Parameter Identification

SSI-DATA, EFDD, and NExT-ERA methods were used for modal parameter estimation [Reynders, 2012]. NExT-ERA and EFDD methods are programmed in MATLAB environment [MATLAB, 2017], and SSI-DATA method is used from a commercial software [ARTeMIS, 2016]. These methods can be categorized into two groups based on the domains they operate. From this perspective, NExT-ERA and SSI-DATA are time domain methods, and EFDD is a frequency domain method. Regardless of how they are classified, these methods assume the followings for the dynamic system to be identified: (i) linearity, (ii) time invariance, and (iii) observability. For more detailed discussions, interested readers can refer to the related literature [Peeters and De Roeck, 2001, Reynders, 2012, Brincker and Ventura, 2015, Rainieri and Fabbrocino, 2014].

5 Damage Observations and Test Results

Detailed visual damage observations were made and documented during quasi-static tests. A summary of these observations at specific drift ratio intervals is given in Table 2 for each frame. In addition, a set of photographs of the tested frames at 0.2% and 3.5% drift ratios are presented in Figure 6 as a complementary information for Table 2. Although detailed damage descriptions at each drift ratio are given in the table, some important characteristics of damage trends for the frames are summarized: For the frame with locked infills, stepped and horizontal cracks were mainly formed at the brick-to-brick interfaces over a large portion of the infill wall due to the sliding mechanism. Numerous and scattered plaster cracks (i.e., no concentration of crack patterns) occurred and no significant brick crushing was observed. On the other hand, for the frame with standard type infills, cracks were concentrated at the corner zones where a biaxial compression-compression stress state occurs due to the lateral in-plane load which results in brick members to crush and spall around the corner zones (i.e., concentration of cracks). Also, it can be said that the standard bricks cause number and width of the cracks induced on the surrounding frame to increase. From this perspective, it can be said that two infilled frames have different damage patterns.

The system identification methods briefly presented above were used with the response data from WN and AV tests. Two different WN excitations, namely with OTT (WN w/Offline) and without OTT (WN wo/Offline), were used for all the frames. The root mean square (RMS) amplitudes of the shaker excitations measured by the accelerometer on the shaker mass (i.e., Sta 8, x-direction) were ~0.46g and ~0.21g for WN wo/Offline and WN w/Offline cases, respectively. Notice that the WN wo/Offline case has more than two times the RMS response amplitude of the WN w/Offline case. Three different tests, namely WN wo/Offline, WN w/Offline, and AV, produced ~0.011g, ~0.004g, and ~4.17E-05g RMS response amplitudes along the in-plane direction (along x-direction) at Sta 4, respectively. These values are almost the same for all three frames. Notice that the AV tests lead to very low level response amplitudes. As a result, it is possible to designate, relatively, WN wo/Offline

data as the “high-level”; WN w/Offline the “medium-level”, and AV data as the “low-level” response cases. Dependence of modal parameter identification results on the level of excitation will be discussed in the following sections.

Table 2 - *Summary of Visual Damage Inspections for Different Frames (F: Frame, I: Infill)*

Drifts (%)		Damage Description		
		F1 (no infill)	F2 (locked infill)	F3 (standard infill)
0.075-0.20	F	Minor flexural cracks on the beam (<0.2 mm). No cracks on column.	Minor cracks on column ends (<0.2 mm). No cracks on beam.	Minor flexural cracks on beam - column joints and column ends (<0.2 mm).
	I		Separation between infill panel - frame interfaces started.	Separation started between infill panel - frame interfaces.
0.25-0.50	F	New beam flexural cracks. Flexural column cracks. Minor cracks on the slab and beam (<0.5 mm).	Flexural cracks on various parts of columns, beam ends and slab (<0.2 mm). Cracks are increased in number.	Shear and flexural cracks arised at various zones of beam and column ends.
	I		Minor diagonal cracks at corner zones. No considerable visible damage on infill.	Diagonal cracks at corner zones. Plaster was spalled due to crushing.
0.75-1.00	F	Moderate damage on frame joints. New minor flexural cracks on beam (<1 mm).	Flexural cracks on columns, beam and slab are increased in number (Crack width < 0.5 mm).	New diagonal shear cracks arised on column ends. Some flexural cracks on beam and column ends propagated.
	I		Frame - infill contact interface started to lost (separation > 1cm). Minor cracks at corner. No considerable crack on infill.	No additional visible cracks. Gap between frame - infill panel became more than 10 mm.
1.40	F	Uplift between foundation - column ends. Moderate flexural cracks on slab and beam/column ends (>2 mm).	New slab cracks appeared.	New flexural cracks arised on beam and column ends. Shear cracks appeared at bottom part of columns.
	I		Shear cracks arised in both diagonal direction. 2 cm gap formed between panel - frame interface. Plaster swelled.	More than 10 mm gap between panel - frame interface. Plaster was spalled due to crushing at corners.
1.75-2.20	F	Uplift between foundation - column ends increased. Moderate - severe flexural cracks on column - beam interfaces (>3 mm).	Moderate - severe frame cracks (> 5 mm).	New flexural cracks arised throughout the beam, on slab and column bottom ends.
	I		Plaster was spalled at corner zone. Irregular horizontal crack formations. In some parts, gap between two brick > 10 mm.	Infill was crushed and spalled only at corner parts. More than 25 mm gap between panel - frame interface.
2.75-3.50	F	Severe flexural damage on frame (>5 mm). Spalling and crushing at base of column concrete. Buckling of reinforcing bars at column bottom ends.	Reinforcing bars became visible and buckled. Concrete was spalled at bottom ends of columns. New frame cracks observed.	Reinforcing bars became visible and buckled. Cracks were propagated at column bottom ends.
	I		Plaster was spalled throughout the wall.	More than 35 mm gap between panel - frame interface. No additional infill wall damage.

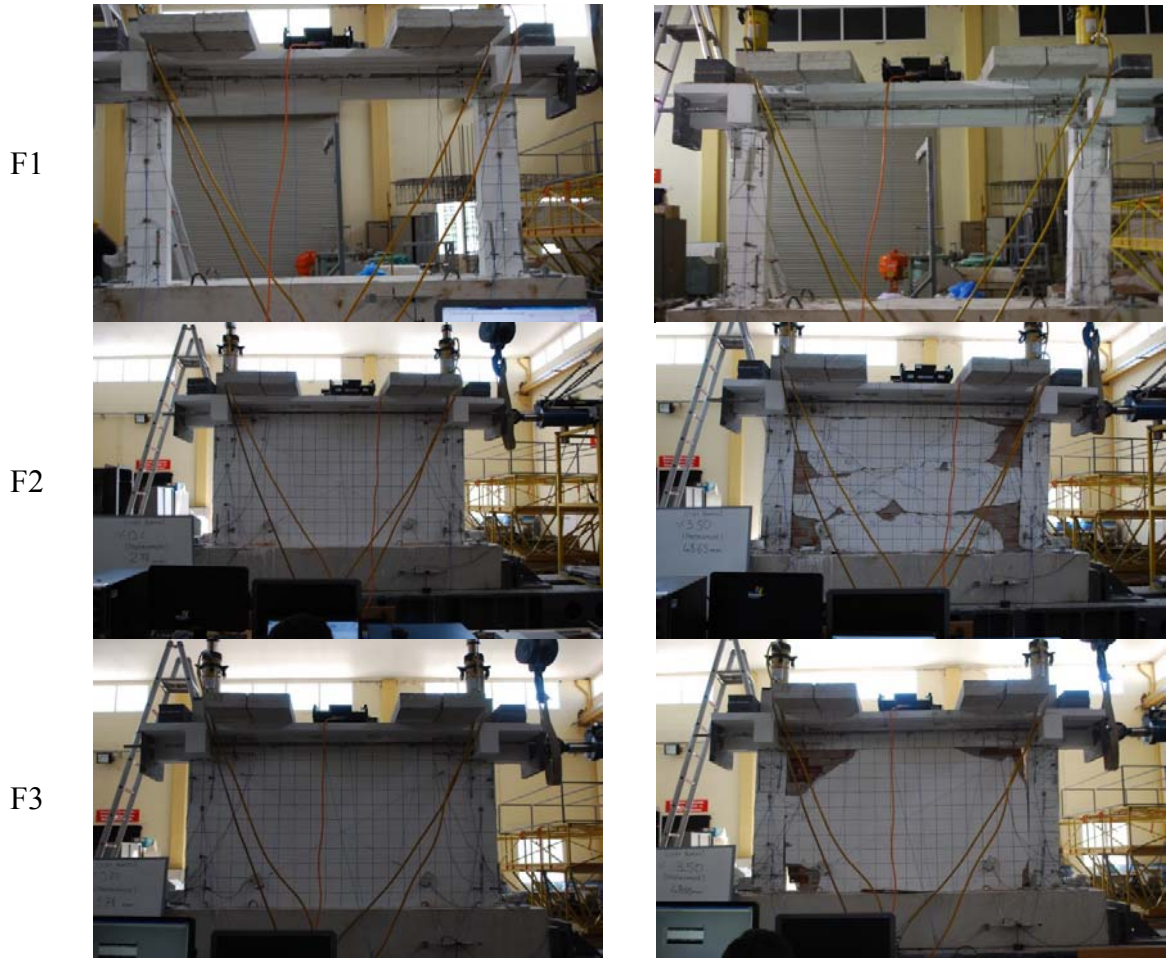

Figure 6 - *Damage States of the Frames at the End of:* (a) *0.2%, and* (b) *3.5% Drift Ratios, respectively*

In this paper, unless otherwise stated, the presented estimation results are from the NExT-ERA method using WN w/Offline test data. The estimated modal parameters belong to the first in-plane (i.e., along x-direction) mode for different frames at progressively increasing damage levels. The estimation results corresponding to the higher modes are not presented at this stage; since the focus has been given to the fundamental mode (the largest contributor to the frames' dynamic response along this direction). Due to setting the shaker's excitation direction along the in-plane direction (x-direction, see Figure 4), the recorded structural response was predominantly along this direction; therefore the WN tests were mainly used to track the changes in the fundamental in-plane mode with respect to gradually increasing structural damage. It must be emphasized that the fundamental modes at different damage states presented here are called the "in-plane modes" due their predominant motions being along the x-direction; but these modes are not purely in-plane modes. In different levels, some identified in-plane modes, at different damage states, are coupled modes, meaning that they have components also along y-(transversal) and z-(vertical) directions. Especially for the infilled frames at lower damage states, the in-plane fundamental modes were not at all purely in-plane modes. As the walls progressively went through more damage, the estimated in-plane mode shapes become more and more in-plane by losing their mode components along

y-, and z-directions. In order to facilitate the discussion of the results, the coupled modes with dominant in-plane components are designated as in-plane modes.

Modal identification results for the fundamental in-plane modes at different damage states using three different excitation types are presented in Figure 7. Here, the selection of the modes at different damage states are done by using stabilization diagrams. These diagrams are helpful tools to be used with parametric system identification methods (e.g., SSI-DATA and NExT-ERA). They are used for determining proper system orders and for distinguishing stable and unstable modes [Peeters and De Roeck, 2001, Zhang *et al.*, 2014]. As an illustrative example, a stabilization diagram is shown in Figure 8 for the WN w/Offline dataset for F1 (the frame wo/infill) at the undamaged state (i.e., 0% drift). The following stability criteria are used to obtain the diagram

$$\left|f_i - f_j\right| / f_j \le 1\% \; ; \qquad \left|\xi_i - \xi_j\right| / \xi_j \le 5\% \; ; \qquad \left|1 - \mathrm{MAC}_{\phi_i,\phi_j}\right| \le 1\% \tag{1}$$

where the estimated frequencies and the damping ratios for models of successive orders are denoted as (f_i, f_j) and (ξi, ξ_j), respectively. $\mathrm{MAC}_{\phi i,\phi j}$ term represents the modal assurance criteria (MAC) of a pair of mode shapes identified for two different models of successive orders [Allemang, 2003]. The symbols shown in the stabilization diagram denote "⊕": a pole with stable frequency, damping, and mode shape, ".d": a pole with stable frequency and damping, ".v": a pole with stable frequency and mode shape, and ".f": a pole with stable frequency only. In the figure, also smoothened and amplitude scaled power spectral density functions (PSDs) are shown which are calculated using the response data recorded at "Sta 3" along x, y, and z-directions from a tri-axial accelerometer. The model order of 14 was chosen for this particular case.

From the results presented in Figure 7, it can be said that the frames subjected to three different excitations, similar frequency values are estimated for a particular damage level and for that particular frame, and as damage increases estimated values become smaller.

Notice that at the same damage level (e.g., 2.2%) for a particular frame, the frequency results from the WN wo/Offline case (relatively a higher level of excitation), are the smallest ones compared to the relatively lower level excitation cases (e.g., AV and WN w/Offline tests), and the highest values being the ones from the AV tests (the lowest level of excitation case). This is due to R/C frames behaving nonlinearly (or quasi-linearly) even at the level of WN wo/Offline case (refer above for their RMS amplitudes).

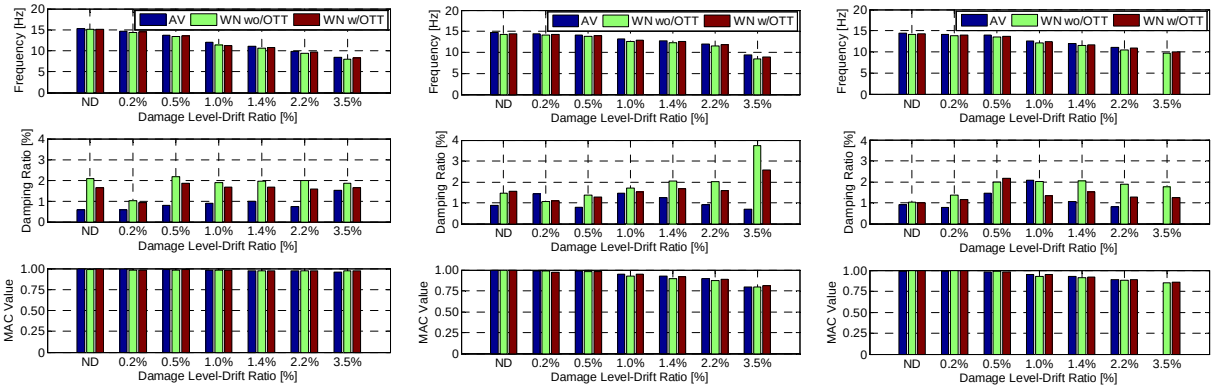

F1 (no infill) *F2 (locked infill)* *F3 (standard infill)*

Figure 7 - *Estimated Modal Parameters for Different Frames Using Different Excitation Types (NExT-ERA Results)*

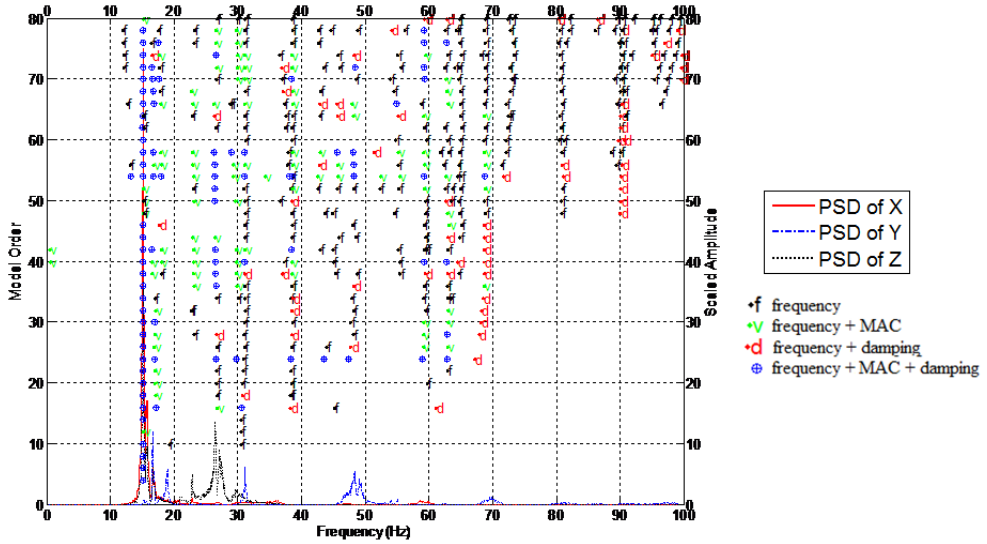

Figure 8 - *Stabilization Diagram of F1 at the Undamaged State (NExT-ERA Results with WN w/Offline Dataset)*

Higher excitation levels, which are expected to widen pre-existing and/or newly emerged cracks in the members, lead to decreased in-plane stiffness which in turn results in smaller frequency estimations. Note that in Figure 7, the modal parameters couldn't be identified using the AV data set at 3.5% damage state for F3. This is due to low signal-to-noise ratio (SNR) seen in this particular data set; but for all the other frames and damage levels, no such problem was observed.

MAC values presented in Figure 7 are calculated between the mode shapes of the undamaged states of F1, F2, and F3 and the different damaged states of the same frames. The MAC values show the changes taking place in mode shapes as structural damage increases. It is clearly seen that the MAC values for F1, F2, and F3 consistently decrease as damage increases indicating that the estimated mode shapes at different damage states differ increasingly more with respect to the mode shapes of the undamaged cases. Notice that the changes in mode shapes are more pronounced for the infilled frames F2 and F3. This is due to the infill wall-frame interaction. The reason for this is that the almost purely in-plane mode remains purely in-plane regardless of damage level for frame F1 (no infill therefore no infill-frame interaction). This results in small variations in MAC estimations. On the other hand, the coupled modes, dominantly seen in the infilled frames at the undamaged and low level damaged states, turn into purely in-plane modes as damage progresses, resulting in significant change in MAC values.

The damping ratio estimations presented in Figure 7 show significant variability among different excitation and frame types, and do not have clear trends that can be used solely as a damage indicator. It is known that in real life measurements, noise always exists and SNR plays an important role in accurate parameter estimation. Specifically, damping is very sensitive to measurement noise and as the noise level increases uncertainty in damping estimations also increases [Bajric *et al.*, 2014, Bajric *et al.*, 2015]. Another peculiarity with damping estimations is the fact that they are amplitude dependent. The damping estimations from the WN data (especially the WN wo/OTT tests which have the largest RMS amplitudes) are consistently higher than the ones estimated from the AV data (which have the smallest RMS amplitudes) for all the frames at all damage states. It should be noted that the lowest

amplitude dependency in damping estimations is observed for F1 (the frame wo/infill) might potentially be indicating that frame-infill interaction plays a role also in damping estimations. In order to investigate the method-to-method variability in estimation results, the recorded response data at different damage states was processed by three different system identification methods. The obtained results are presented in Figure 9. The MAC values shown in the figures are found between the undamaged mode shapes (using the WN w/Offline tests and estimated by NExT-ERA method) and the damaged ones (using the WN w/Offline tests and estimated by SSI-Data and EFDD methods) for different frames. It can be said that frequency estimations and MAC values by different methods are very similar for each damage state (i.e., negligible differences), therefore the estimated values are independent of the method used). For the damping estimations, it can be said that NExT-ERA and SSI-DATA methods give somewhat similar results; but the overall match for the damping estimations among the methods is not as good as the frequency and mode shape estimations. The damping results by EFDD method differ more from the results obtained by the other two methods. This higher variability in damping estimations by EFDD method can be attributed to the subjectiveness of the peak-picking process. An increasing or a decreasing trend for the damping ratio estimations, as observed for the frequency and mode shape estimations at the level of excitations considered in this study, cannot be observed as damage increases. Nevertheless, a slight increasing trend in damping estimations is noticeable as the drift ratio increases (e.g., F2). Modal parameter estimations for all the frames are shown comparatively in Figure 10 as a function of damage level. For the undamaged state, the natural frequencies of frames F1 to F3 are identified as 15.11 Hz, 14.43 Hz and 14.20 Hz, respectively. It is expected that the existence of infills would have stiffening effect along the in-plane direction and therefore the frequencies of the in-plane modes would increase; but it is interesting to note that F1 (the frame wo/infill) has the highest natural frequency among the frames tested. This may be considered as a counter-intuitive result at a first glance; but it should be emphasized that the in-plane mode shapes of the frames w/infill walls are coupled modes (i.e., the modes for these frames are not purely in-plane) especially at low damage levels (e.g., at the ND and 0.2% drifts) whereas F1 has purely in-plane mode shapes for all drift cases (Figure 11). The coupled nature of the in-plane modes for the infilled frames is due to frame-infill interaction. Therefore, a direct comparison of the estimated frequencies for the frames with and without infills at low damage levels may be misleading.

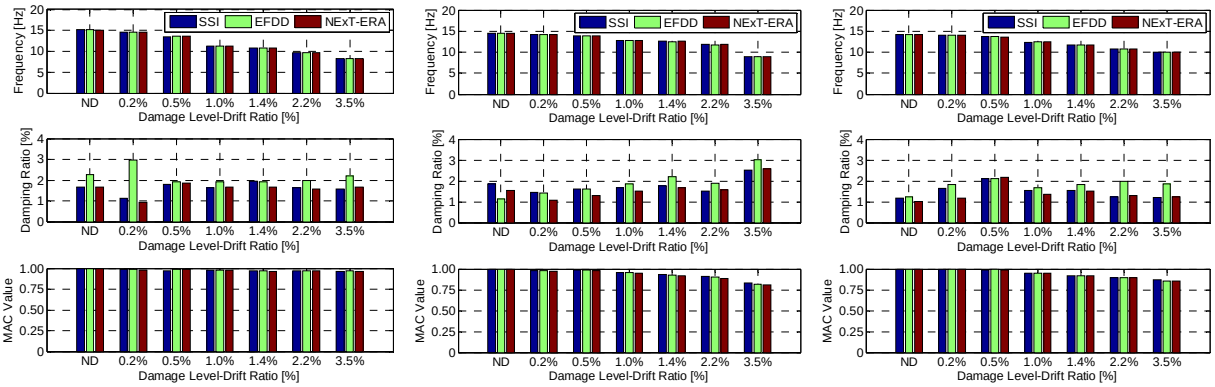

F1 (no infill) *F2 (locked infill)* *F3 (standard infill)*

Figure 9 - *Estimated Modal Parameters for Different Frames by Different System Identification Methods (WN w/Offline Dataset)*

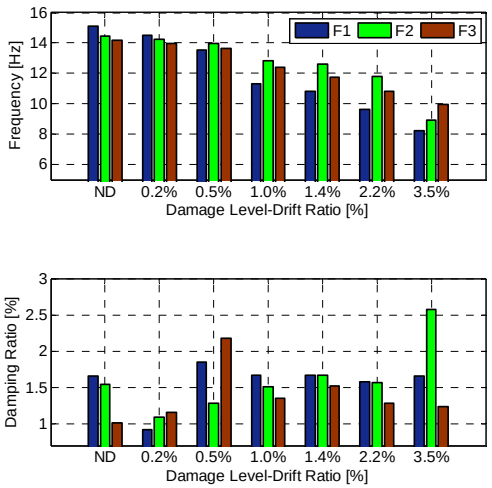

Figure 10 - *Modal Parameter Estimation Results for the Frames as a Function of Damage Level (NExT-ERA Results with WN w/Offline Dataset)*

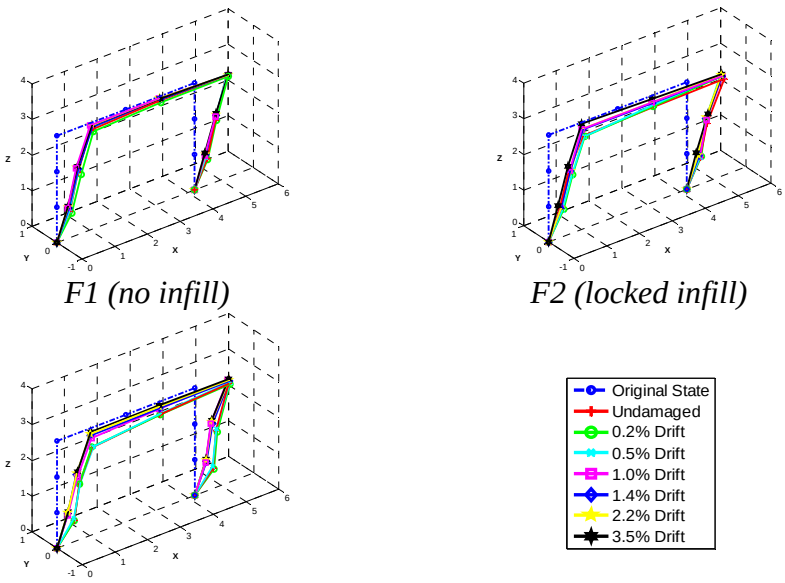

F1 (no infill) *F2 (locked infill)*

F3 (standard infill)

Figure 11 – *Evolution* of *Mode Shapes as Structural Damage Increases*

At the undamaged state, all frames w/infills have similar frequencies for the pre-dominantly in-plane modes (with coupled out-of-plane components). As these frames get damaged, they start to differentiate from each other depending on the infill condition, this starts at around 0.5% drift. It is clear from the figure that a steady decrease takes place in the frequency estimations for all the frames as damage increases; but it is clear that the lateral stiffness of the frame wo/infill (F1) decreases at a faster rate than the frames with infills. This is not a surprising result: although the infill walls get damaged they still contribute significantly to the in-plane stiffness especially at the dynamic excitation levels attained in this study. Also, it is important to note that the decreasing trend in the frequency estimations for the frame with locked bricks (F2) is slower than the other two. This might possibly be indicating that the additional damage that might be induced by frame-infill interaction is less severe for F2 (due to mild panel action) than F3 (the frame w/ standard bricks). Another reason for that would

be the sliding mechanism of the locked bricks: bricks sliding on top of each other make this type of wall more resilient to structural damage. At 3.5% drift ratio, the identified frequencies for the frames F1, F2, and F3 are 8.23 Hz, 8.94 Hz and 9.94 Hz, respectively. The percentage changes in the frequencies with respect to the undamaged states are calculated as 45% (F1, wo/infill), 38% (F2, w/locked infill) and 30% (F3, w/standard infill). These results show that the frames with the locked type infill (F2) and without infill (F1) are somewhat similar. The frame with standard bricks (F3) shows smaller frequency change between the undamaged (ND) and the highest damaged (3.5% drift) states. Moreover as shown in Figure 10, it can be said that at the excitation level (i.e., WN w/Offline) attained for these tests, the damping ratio estimations show no clear trend both for damage level and infill condition.

Based on the plots presented in Figure 11, it should be emphasized that as structural damage increases y- and z-components of the in-plane modes for F2 and F3 start to disappear. The modes estimated at higher damage levels (approx. 1.0% and beyond) become almost perfectly in-plane. This result indicates that the effect of infills on the mode shape estimations diminish as damage increases. Figure 12 shows the polar plot representations of the estimated mode shapes with complex components. These plots show the level of non-classical damping in the frames. Based on the results, it can be said that the mode shapes are classically damped (characterized by negligible complex parts) because the vector components are almost perfectly collinear and aligned along the real axis. This also serves as a justification in plotting the estimated mode shapes, which have complex components, using only their real parts (Figure 11). It can also be said that the damage level does not change the classically damped nature of the modes. Figure 11 shows that as the structural damage increases, the in-plane mode shapes go through very small changes. This observation can be used to justify that as damage increases, the effective modal masses corresponding to the fundamental in-plane modes remain unchanged for different frames. With this assumption, the stiffness degradations corresponding to the in-plane modes with respect to the undamaged case can be approximated by the following equation

$$SD_i^j\ (\%) = \frac{\left(f_{ND}^j\right)^2 - \left(f_{D,i}^j\right)^2}{\left(f_{ND}^j\right)^2} \tag{2}$$

where f_{ND}^j j = F1, F2, F3 and $f_{D,i}^j$ are the identified frequencies for a particular frame (j) at the undamaged and various damaged levels (i=ND, 0.2%, 0.5%, 1.0% etc.), respectively.

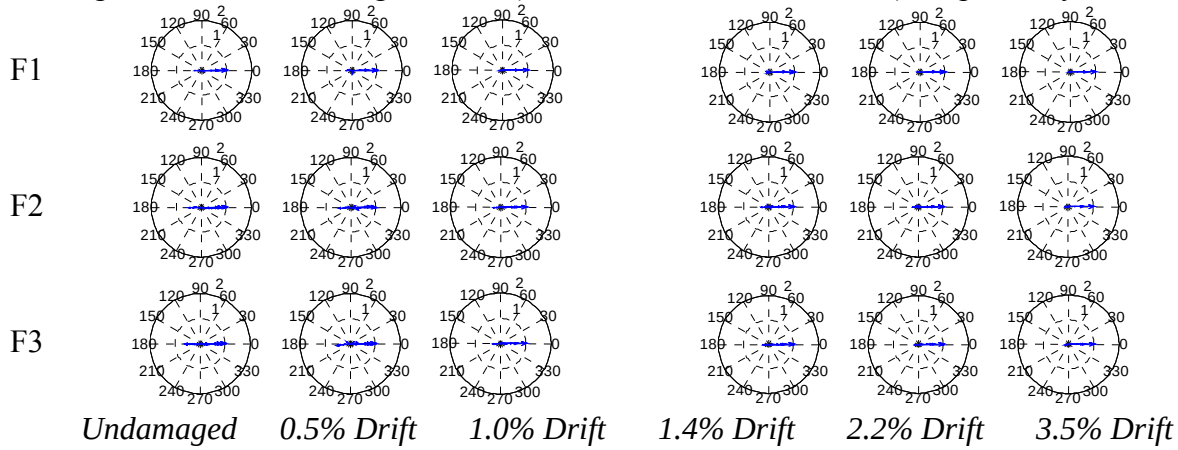

Figure 12 - *Polar Plot Representations of Mode Shapes*

The stiffness degradations calculated using the above equation at different drift levels for different frames are matched with the detailed visual damage inspections (refer to Table 2). The results are aggregated into three dimensional plots and are presented in Figures 13 to 15 for frames F1, F2, and F3, respectively. In these figures, damage types are categorized for column (subplot a), beam (subplot b), and infill (subplot c) members in three distinct groups, and subplots (d) show the zones where damages are concentrated. The bars with red colors indicate that a particular damage type (as indicated on the longitudinal axis) occurred for the first time or that damage type increased significantly at that particular drift ratio (as indicated on the transversal axis). The bars with yellow colors indicate that no significant change in the existing damage type occurred and the bars with green colors indicate that a particular damage type has not yet occurred at that drift ratio. The bars with gray colors indicate that the corresponding member damages do not exist for that frame (e.g., there is no wall in F1, therefore Figure 13(c) is all in gray color). These figures are useful in determining what damage type (also its extent, and its location) has more pronounced effect on the stiffness degradation as a function of increasing structural damage. Note that the stiffness degradation values are calculated using the frequency estimations.

For F1 (the frame wo/infill) in Figure 13, the damages at beam ends due to the flexural action were effective until 0.2% drift ratio, and these damages resulted in ~8% stiffness degradation. With increasing drift ratio, up to 1.0%, the damage at column ends started to be more pronounced in loss of in-plane stiffness. The largest change in stiffness degradation (~25%) was observed within the 0.5%-1.0% drift ratio interval due to mainly column damages (Figure 13(a), damage types 1a, 2a, and 3a). Towards the end of the test, the separation at the column-foundation interface can be seen as the critical factor in stiffness degradation.

For F2 (the frame w/locked infill) in Figure 14, column and infill damages were the defining factors for stiffness degradation until 0.2% drift ratio. The first significant change in the stiffness degradation was observed between 0.5%-1.0% drift interval due to infill (e.g., concentrated cracks at the corner zones, distributed horizontal cracks) and various column damages. The largest change (~29%) was observed between 2.2%-3.5% drift ratio interval due to separation at the frame-infill interface and various column damages (Figure 14(c), damage types 6-7, Figure 14(a), damage types 11a and 11b etc.).

For F3 (the frame w/standard infill) in Figure 15, various types of column cracks, frame-infill separation, and cracks at the corner zones of the infill wall are the main damage types responsible for the stiffness degradation seen within the 0.5%-1.0% drift ratio interval. The largest change in the stiffness degradation (~16%) was also observed within this interval (main damage type for this degradation could not be captured using the damage observations). Within the drift ratios following this range, beam and infill member damages started to substantially increase, however they did not impose a sudden change in the stiffness degradation (i.e., a smoother, more gradual change has been observed for F3 also confirmed by the changes in the frequency estimations).

The stiffness degradation values calculated at the ultimate damage state (i.e., 3.5%) are 70%, 62%, and 51% for the frames F1 (wo/infill), F2 (w/locked infill) and F3 (w/standard infill), respectively. It should be emphasized here that the quasi-static tests allowed performing detailed damage observations, the dynamic tests allowed stiffness degradations to be calculated using the modal parameter estimations. By combining static and dynamic tests, it was possible to match different damage types (from static tests) with stiffness degradations obtained through the frames' dynamic response (from dynamic tests).

1a) Flexural cracks at column bottom ends.
2a) Flexural cracks at column top ends.
3a) Flexural cracks at column central zone.
1b) Shear cracks at column bottom ends.
2b) Shear cracks at column top ends.
3b) Shear cracks at column central zone.
4a) Shear cracks at column-beam joint region.
11a) Crushing of cover concrete at left column bottom end.
11b) Crushing of cover concrete at right column bottom end.
12a) Uplift between left column and foundation.
12b) Uplift between right column and foundation.
13) Reinforcements at column bottom ends become visible.
15) Buckling of reinforcements at column bottom ends.
18) Rupture of reinforcement at column bottom ends.
22) 2 mm crack width at column ends.
23) 5 mm crack width at column ends.

4b) Flexural cracks at beam-column joint region.
5a) Flexural cracks at beam ends.
5b) Flexural cracks at beam central region.
10) Flexural cracks at slab.
14) Reinforcements at beam ends become visible.
16) Buckling of reinforcement at beam ends.
17) Rupture of reinforcement at beam ends.
19) 2 mm crack width at beam ends.
20) 5 mm crack width at beam ends.
21) 10 mm crack width at beam ends.

6) Separation starts between infill wall – beam interface.
7) Separation starts between infill wall – column interface.
6-7) Frame-infill interface separation.
8a) Horizontal shear cracks at central and edge zones.
8b) Diagonal shear cracks at central and edge zones.
8c) Cracks at upper and lower side of infill.
9a) Cracks at infill corner (a).
9b) Cracks at infill corner (b).
9c) Cracks at infill corner (c).
9d) Cracks at infill corner (d).
8-9-a) Crushing and spalling of plaster.
8-9-b) Spalling of infill wall.

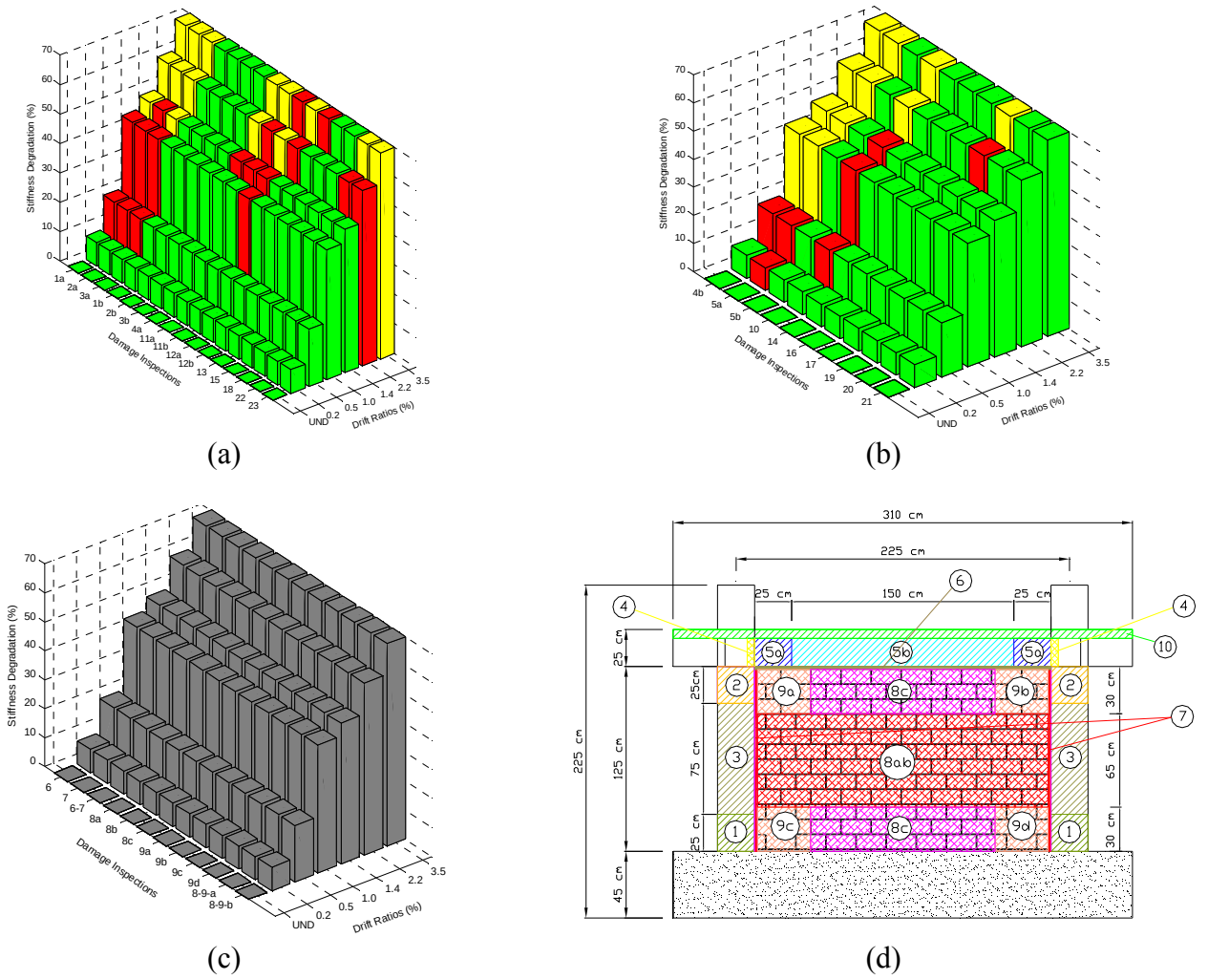

Figure 13 - *Combined Stiffness Degradation-Visual Damage Inspections Plots for F1: (a) Column, (b) Beam, (c) Infill Wall Members, and (d) Approximate Zonation of Different Damage Types*

1a) Flexural cracks at column bottom ends.
2a) Flexural cracks at column top ends.
3a) Flexural cracks at column central zone.
1b) Shear cracks at column bottom ends.
2b) Shear cracks at column top ends.
3b) Shear cracks at column central zone.
4a) Shear cracks at column-beam joint region.
11a) Crushing of cover concrete at left column bottom end.
11b) Crushing of cover concrete at right column bottom end.
12a) Uplift between left column and foundation.
12b) Uplift between right column and foundation.
13) Reinforcements at column bottom ends become visible.
15) Buckling of reinforcements at column bottom ends.
18) Rupture of reinforcement at column bottom ends.
22) 2 mm crack width at column ends.
23) 5 mm crack width at column ends.

4b) Flexural cracks at beam-column joint region.
5a) Flexural cracks at beam ends.
5b) Flexural cracks at beam central region.
10) Flexural cracks at slab.
14) Reinforcements at beam ends become visible.
16) Buckling of reinforcement at beam ends.
17) Rupture of reinforcement at beam ends.
19) 2 mm crack width at beam ends.
20) 5 mm crack width at beam ends.
21) 10 mm crack width at beam ends.

6) Separation starts between infill wall – beam interface.
7) Separation starts between infill wall – column interface.
6-7) Frame-infill interface separation.
8a) Horizontal shear cracks at central and edge zones.
8b) Diagonal shear cracks at central and edge zones.
8c) Cracks at upper and lower side of infill.
9a) Cracks at infill corner (a).
9b) Cracks at infill corner (b).
9c) Cracks at infill corner (c).
9d) Cracks at infill corner (d).
8-9-a) Crushing and spalling of plaster.
8-9-b) Spalling of infill wall.

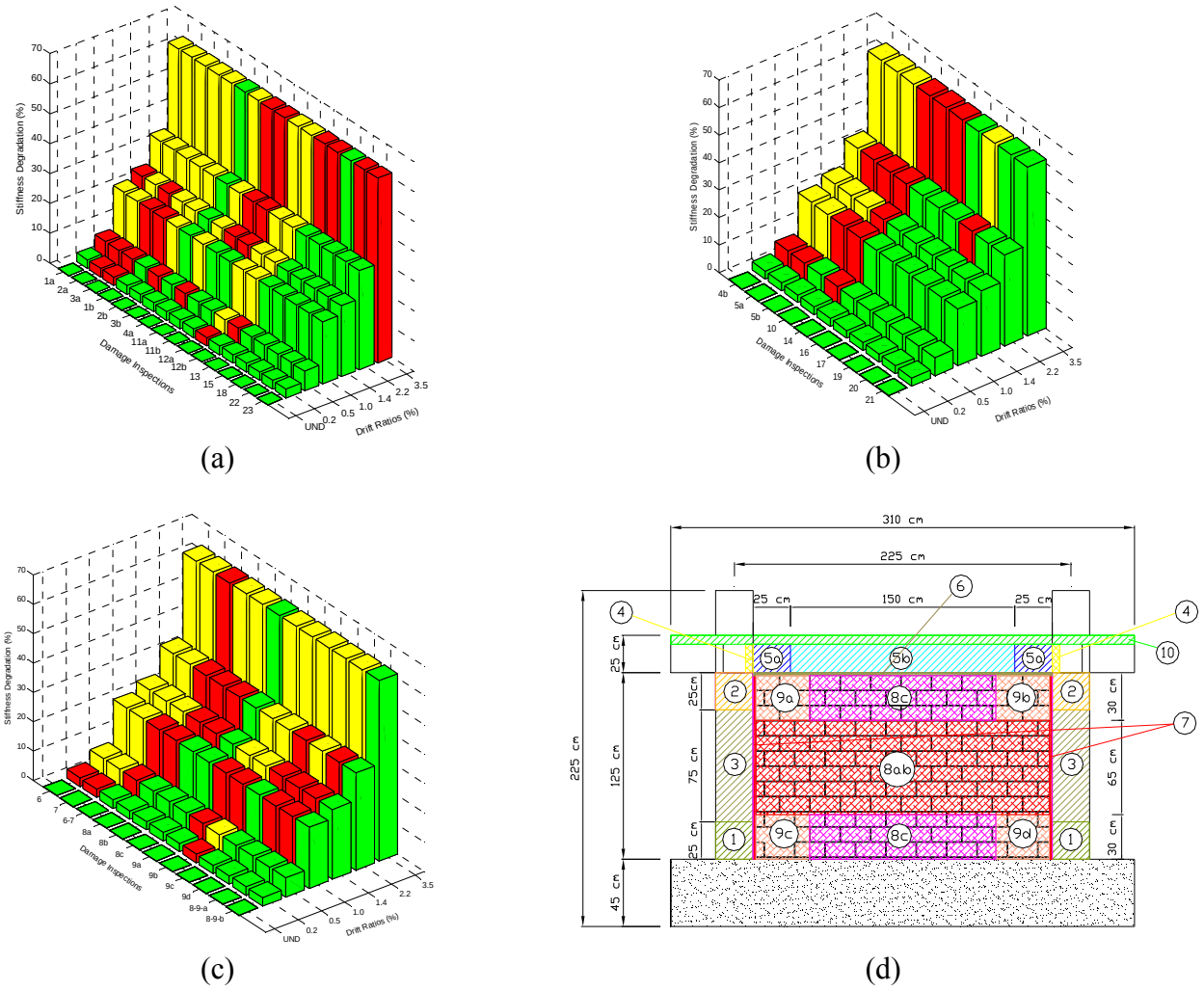

Figure 14 - *Combined Stiffness Degradation-Visual Damage Inspections Plots for F2: (a) Column, (b) Beam, (c) Infill Wall Members, and (d) Approximate Zonation of Different Damage Types*

1a) Flexural cracks at column bottom ends.
2a) Flexural cracks at column top ends.
3a) Flexural cracks at column central zone.
1b) Shear cracks at column bottom ends.
2b) Shear cracks at column top ends.
3b) Shear cracks at column central zone.
4a) Shear cracks at column-beam joint region.
11a) Crushing of cover concrete at left column bottom end.
11b) Crushing of cover concrete at right column bottom end.
12a) Uplift between left column and foundation.
12b) Uplift between right column and foundation.
13) Reinforcements at column bottom ends become visible.
15) Buckling of reinforcements at column bottom ends.
18) Rupture of reinforcement at column bottom ends.
22) 2 mm crack width at column ends.
23) 5 mm crack width at column ends.

4b) Flexural cracks at beam-column joint region.
5a) Flexural cracks at beam ends.
5b) Flexural cracks at beam central region.
10) Flexural cracks at slab.
14) Reinforcements at beam ends become visible.
16) Buckling of reinforcement at beam ends.
17) Rupture of reinforcement at beam ends.
19) 2 mm crack width at beam ends.
20) 5 mm crack width at beam ends.
21) 10 mm crack width at beam ends.

6) Separation starts between infill wall – beam interface.
7) Separation starts between infill wall – column interface.
6-7) Frame-infill interface separation.
8a) Horizontal shear cracks at central and edge zones.
8b) Diagonal shear cracks at central and edge zones.
8c) Cracks at upper and lower side of infill.
9a) Cracks at infill corner (a).
9b) Cracks at infill corner (b).
9c) Cracks at infill corner (c).
9d) Cracks at infill corner (d).
8-9-a) Crushing and spalling of plaster.
8-9-b) Spalling of infill wall.

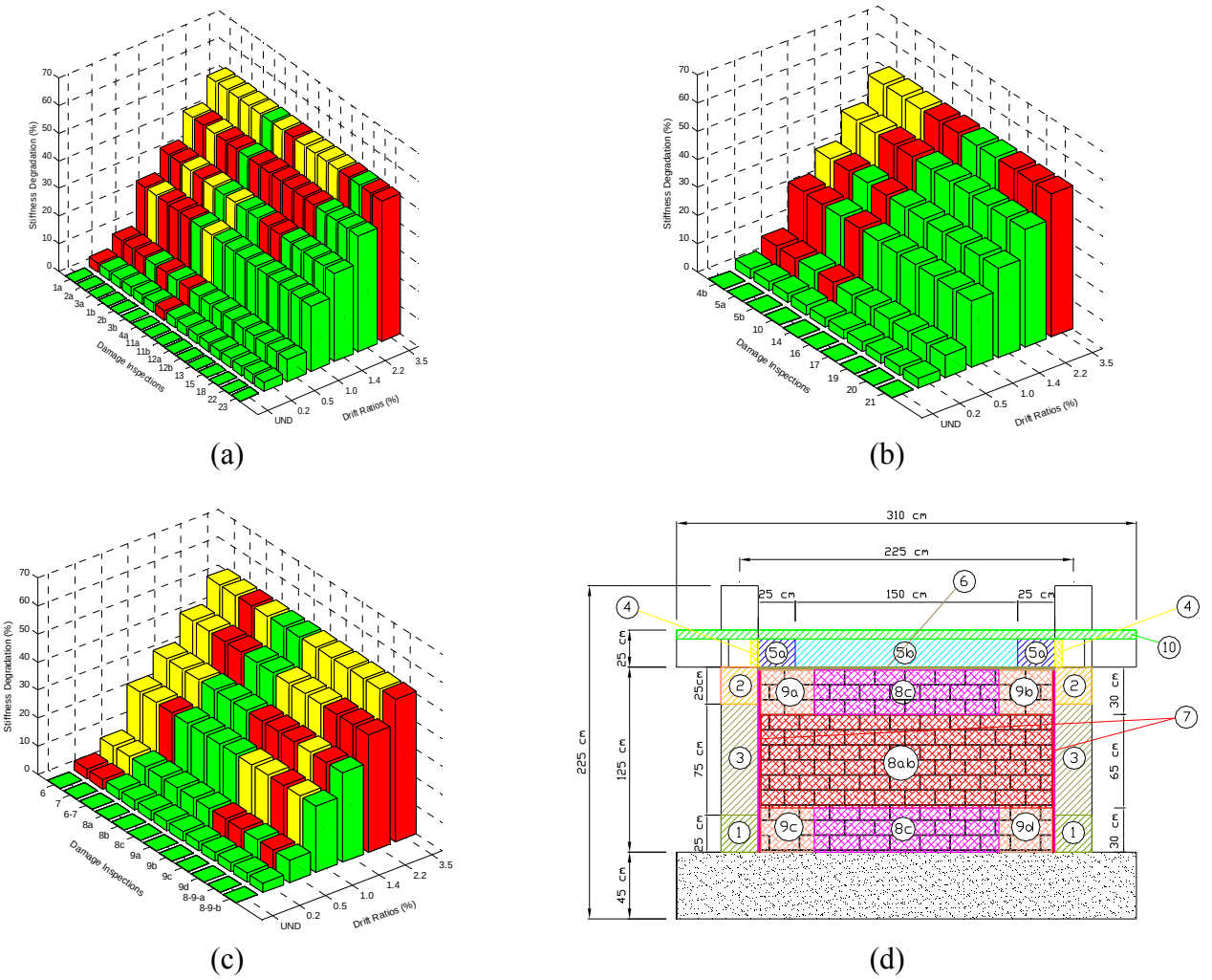

Figure 15 - *Combined Stiffness Degradation-Visual Damage Inspections Plots for F3: (a) Column, (b) Beam, (c) Infill Wall Members, and (d) Approximate Zonation of Different Damage Types*

6 Conclusions

In this study half-scale, single-bay, single-story three R/C frames with different infill conditions were tested under single-cycle quasi-static loading along the frames' in-plane direction. At the pre-determined drift levels, WN and AV tests were performed on the frames. In order to perform modal parameter identification at different damage levels, three different system identification methods, namely, SSI-DATA, NExT-ERA, and EFDD are used.

The findings of the study that can be generalized are as follows: (i) the results of three different output-only system identification methods are very close to each other for frequency and mode shape estimations under different excitation conditions. The methods used in this study can identify all modal parameters of the R/C frames at different damage levels using WN data whereas it is difficult to process the AV datasets by EFDD method due to the corresponding data sets' low SNR characteristics. (ii) The identified frequencies are affected by the excitation level. This shows that the frequency estimations are affected by the nonlinear behavior of R/C frames even by small changes in the excitation level. (iii) For the damping estimations, it can be said that NExT-ERA and SSI-DATA methods give somewhat similar results; but the overall consistency of the damping estimations among different methods is not as good as the frequency and mode shape estimations. The damping results by EFDD method are more different than the values estimated by the other two methods. This higher variability observed in damping estimations by EFDD method can be attributed to the subjectiveness of the peak-picking process. (iv) The decreasing trend in the frequency estimations with respect to increasing structural damage for the frame with locked bricks is slower than the other two. This may possibly be indicating that the extra damage that may be induced by frame-infill interaction is less severe for the frame w/locked infills, due to mild panel action, than for the frame w/standard infills. (v) The changes in MAC values as the structural damage increases are more pronounced for the infilled frames. This can be attributed to the infill wall–frame interaction. The effect of infills to the mode shapes diminish as infill damage increases. The damage level does not change the classically damped nature of the mode shapes. (vi) The identified damping ratios exhibit large variability, and do not follow a clear trend that can be associated with increasing structural damage. Nevertheless, a slight increasing trend in damping estimations is noticeable as the structural damage increases (especially for the frame with locked bricks). (vii) Damping ratio estimations are amplitude dependent and are sensitive to SNR. The AV data results in lower and the WN data results in higher damping estimations. Frame-infill interaction, which is more pronounced under higher level excitation, affects damping ratio estimations. These results are applicable for R/C frames with infill walls loaded along their in-plane directions only, dynamic characterization of similar R/C frames with infills under bi-directional loading (i.e., loaded by simultaneous in-plane and out-of-plane loads) should be addressed in the future.

8 Acknowledgements

The authors greatly acknowledge the financial support provided by The Scientific and Technological Council of Turkey (TUBITAK) under the grant #112M203. Authors are also thankful to I. Serkan Misir, Carmen Amaddeo, Sadik Can Girgin, Muhammed Emin Demirkiran, Ozgur Girgin, Onur Baskaya, Ustun Can Meric, Gokhan Okudan, Mazlum Yagız,

Umut Candan, Fahri Tokgoz, Filiz Vargun, Mustafa Uslu, Bayram Kaya, Samet Goymen, Duygu Senol, Inci Terkan for their help in test preparations.

References

ACI 374.1-05 (2005). Acceptance criteria for moment frames based on structural testing and commentary. American Concrete Institute, Farmington Hills, Detroit, Michigan, USA.

Allemang, R. J. (2003). The modal assurance criterion–twenty years of use and abuse. Sound and Vibration, 37(8):14-23.

ARTeMIS Extractor Pro (2016). Structural Vibration Solutions, Aalborg, Denmark.

Astroza, R., Ebrahimian, H., Conte, J. P., Restrepo, J. I. and Hutchinson, T. C. (2016). System identification of a full-scale five-story reinforced concrete building tested on the NEES-UCSD shake table. Structural Control and Health Monitoring, 23(3):535-559.

Bajric, A., Brincker, R. and Georgakis, C. T. (2014). Evaluation of damping using time domain oma techniques, Proc. of 2014 SEM Fall Conference and International Symposium on Intensive Loading and Its Effects, Beijing, China.

Bajrić, A., Georgakis, C. T. and Brincker, R. (2015). Evaluation of damping using frequency domain operational modal analysis techniques. In: Caicedo, J., Pakzad, S., editors, Dynamics of Civil Structures, volume 2, Springer International Publishing, pp. 351-355.

Belleri, A., Moaveni, B. and Restrepo, J. I. (2014). Damage assessment through structural identification of a three-story large-scale precast concrete structure. Earthquake Engineering & Structural Dynamics, 43(1):61-76.

Brincker, R. and Ventura, C. (2015). Introduction to Operational Modal Analysis. John Wiley & Sons, Chichester, UK.

Doebling, S. W., Farrar, C. R. and Prime, M. B. (1998). A summary review of vibration-based damage identification methods. Shock and Vibration Digest, 30(2):91-105.

Donà, M., Minotto, M., Saler, E., Tecchio, G. and Porto da, F. (2017). Combined in-plane and out-of-plane seismic effects on masonry infills in RC frames. Ingegneria Sismica, 34(3): 157-174.

Ji, X., Fenves, G. L., Kajiwara, K. and Nakashima, M. (2010). Seismic damage detection of a full-scale shaking table test structure. Journal of Structural Engineering, 137(1):14-21.

Lima, C., Martinelli, E. and Faella, C. (2017). Simplified nonlinear static procedures for seismic assessment of masonry infilled RC structures. Ingegneria Sismica, 34(3): 139-156.

Luco, J. E., Ozcelik, O. and Conte, P. (2010). Acceleration tracking performance of the UCSD-NEES shake table. Journal of Structural Engineering, 136(5):481-490.

MATLAB (2017). The MathWorks Inc, Natick, Massachusetts, USA.

Misir, S., Ozcelik, O., Girgin, S. C. and Kahraman, S. (2012). Experimental work on seismic behavior of various types of masonry infilled rc frames. Structural Engineering and Mechanics, 44(6):763-774.

Moaveni, B., He, X., Conte, J. P., Restrepo, J. I. and Panagiotou, M. (2010). System identification study of a 7-story full-scale building slice tested on the UCSD-NEES shake table. Journal of Structural Engineering, 137(6):705-717.

Moaveni, B., Stavridis, A., Lombaert, G., Conte, J. P. and Shing, P. B. (2012). Finite-element model updating for assessment of progressive damage in a 3-story infilled rc frame. Journal of Structural Engineering, 139(10):1665-1674.

Mota, M. (2011). Shake table acceleration tracking performance impact on dynamic similitude. PhD Dissertation, Faculty of Drexel University, Philadelphia, USA.

Ozcelik, O., Misir, I. S., Amaddeo, C., Yucel, U. and Durmazgezer, E. (2015). Modal identification results of quasi-statically tested rc frames at different damage levels. In: Mains, M., editor, Topics In Modal Analysis, volume 10, Springer International Publishing, pp. 215-226.

Peeters, B. and De Roeck, G. (2001). Stochastic system identification for operational modal analysis: a review. Journal of Dynamic Systems, Measurement, and Control, 123(4):659-667.

Rainieri, C. and Fabbrocino, G. (2014). Operational Modal Analysis of Civil Engineering Structures. Springer, New York, USA.

Reynders, E. (2012). System identification methods for (operational) modal analysis: review and comparison. Archives of Computational Methods in Engineering, 19(1):51-124.

Sohn, H., Farrar, C. R., Hemez, F. M., Shunk, D. D., Stinemates, D. W., Nadler, B. R. and Czarnecki, J. J. (2003). A review of structural health monitoring literature: 1996-2001. Report No: LA-13976-MS, Los Alamos National Laboratory, USA.

Stavridis, A., Koutromanos, I. and Shing, P. B. (2012). Shake-table tests of a three-story reinforced concrete frame with masonry infill walls. Earthquake Engineering & Structural Dynamics, 41(6):1089-1108.

Thoen, B. K. and Laplace, P. N. (2004). Offline tuning of shaking tables, Proc. of the 13th World Conference on Earthquake Engineering, Vancouver, Canada.

Twitchell, B. S. and Symans, M. D. (2003). Analytical modeling, system identification, and tracking performance of uniaxial seismic simulators. Journal of Engineering Mechanics, 129:1485-1488.

Yucel, U. (2014). Developing offline-tuning technique to be used for damage level assessment of a model frame type structure and application of system identification methods. MSc Dissertation, The Graduate School of Natural and Applied Sciences, Dokuz Eylul University, Izmir, Turkey.

Zhang, G., Ma, J., Chen, Z. and Wang, R. (2014). Automated eigensystem realisation algorithm for operational modal analysis. Journal of Sound and Vibration, 333(15):3550-3563.

ingegneria sismica
International Journal of Earthquake Engineering
Anno XXXV – Num.4

IDENTIFICAZIONE MODALE DEL DANNEGGIAMENTO PROGRESSIVO DI TELAI IN CEMENTO ARMATO CON DIVERSE TIPOLOGIE DI TAMPONATURE

Ozgur Ozcelik[1,2], Umut Yucel[1], Erkan Durmazgezer[1]

[1]Department of Civil Engineering, Dokuz Eylul University, Izmir, Turkey

[2]Currently a Researcher at Department of Structural Engineering, University of California, San Diego

SUMMARY: *In questo articolo, vengono presentati i risultati dell'analisi modale operazionale di tre telai in cemento armato (CA), ad un piano ed una campata, con tre diverse tipologie di tamponature.*

I telai sono stati testati nel loro piano con dei cicli di carico quasi-statico. Per ogni prefissato spostamento sono stati condotti dei test, in condizioni di vibrazioni ambientali, con lo scopo di identificare i parametri modali. I risultati ottenuti dall'analisi modale operazionale sono stati confrontati con i risultati ottenuti dall'esaustiva analisi visiva del danneggiamento. Lo scopo di questo articolo e' (i) stimare l'evoluzione dei parametri modali valutati in funzione dell'aumento del danneggiamento strutturale, (ii) valutare la performance dei diversi metodi output-only di identificazione dei parametri modali nel caso in cui si abbaino telai danneggiati, (iii) valutare i risultati dei parametri modali in relazione all'uso di diverse tipologie di azioni ed al variare della loro ampiezza massima, (iv) la relazione tra il danneggiamento delle diverse tipologie di tamponature ed i parametri modali ottenuti tramite l'analisi modale operazionale.

KEYWORDS: *telai in cemento armato, test quasi-statici, telai con tamponature, shaker test lineari, identificazione strutturale dei parametri modali, analisi modale operazionale.*

Corresponding author: Ozgur Ozcelik, Department of Civil Engineering, Dokuz Eylul University, Turkey.
Email: ozgur.ozcelik@deu.edu.tr